A steric pore-flow model to predict the transport of small and uncharged solutes through a reverse osmosis membrane

Revised manuscript submitted to

Environmental Science: Water Research and Technology

December 2017

Haruka Takeuchi [a], Hiroaki Tanaka [a], Long D. Nghiem [b], Takahiro Fujioka [c,*]

[a] *Research Center for Environmental Quality Management, Kyoto University, Shiga 520-0811, Japan*

[b] *Strategic Water Infrastructure Laboratory, School of Civil Mining and Environmental Engineering, The University of Wollongong, NSW 2522, Australia*

[c] *Water and Environmental Engineering, Graduate School of Engineering, Nagasaki University, 1-14 Bunkyo-machi, Nagasaki 852-8521, Japan*

* Corresponding author: Takahiro Fujioka, Email: tfujioka@nagasaki-u.ac.jp, Ph +81 095 819 2695

Abstract

This study proposed a new approach to apply the steric pore-flow model to predict the rejection of eight *N*-nitrosamines and seven VOCs that are of great concern in potable water reuse through an RO membrane. In this approach, solute rejection is predicted by estimating the free-volume hole-size. The free-volume hole-radius was determined with pure water permeability of a membrane and a single reference compound − *N*-nitrosodimethylamine (NDMA) − by minimizing the variance between the experimentally obtained and calculated NDMA rejection values at the permeate flux of 20 L/m^{2}h. The obtained free-volume hole-radius of ESPA2 RO membrane was 0.348 nm, which was larger than the value previously determined by positron annihilation lifetime spectroscopy (PALS) analysis (0.289 nm). The model incorporated with the estimated free-volume hole-radius could accurately predict the rejection of eight *N*-nitrosamines under a range of permeate flux (2.6–20 L/m^{2}h). The model was also validated using experimentally obtained VOC rejection values. The predicted VOC rejections at the permeate flux of 20 L/m^{2}h were almost identical to their experimentally obtained rejections. However, VOC rejection prediction at a lower permeate flux was less accurate. Further improvement and validation of the model with a variety of trace organic chemicals is required to allow for a more accurate prediction. The model was also validated using the membrane free-volume hole-radius value previously obtained from PALS analysis. Using PALS data resulted in some over-prediction. The results suggest that PALS analysis cannot allow for model prediction unless additional adjustment is provided to improve the prediction accuracy.

Keywords: *N*-nitrosodimethylamine (NDMA); *N*-nitrosamines; potable water reuse; reverse osmosis; volatile organic compounds.

1. Introduction

Prolonged droughts and the increase in water use have prompted water utilities and authorities in many regions around the world to consider potable water reuse. Potable water reuse is the reclamation of treated wastewater to augment drinking water supply. Water quality requirements for potable water reuse are very stringent. As a result, most water reclamation plants for potable water reuse have adopted reverse osmosis (RO) membrane technology as a key barrier to ensure adequate removal of trace organic chemicals (TrOCs) that are known to occur ubiquitously in treated wastewater.[1–4] However, a few small and neutral TrOCs can readily permeate through RO membranes.[5–7] Examples of these TrOCs are *N*-nitrosamines including *N*-nitrosodimethylamine (NDMA) and volatile organic compounds (VOCs).[8–10] The rejection of these small and neutral TrOCs by RO membranes can vary significantly from negligible to 86% for NDMA[8] and 43-63% for some VOCs.[9] Due to the low and highly variable removal of these TrOCs by RO membranes, a subsequent treatment process such as UV-based advanced oxidation process is often introduced to comply with their guideline or maximum permissible concentration in the final product water intended for reuse purposes.[1,11,12] Thus, it is envisaged that ability to predict and simulate the removal of NDMA and other small and neutral TrOCs by RO membranes can be particularly useful for process optimization.

There are two major approaches for describing the transport of solutes through RO membranes namely irreversible thermodynamics and pore-flow models.[13] In the irreversible thermodynamics model, the membrane is considered as a black box, in which solute and solvent first partition to then diffuse through at different rates.[14,15] These assumptions are consistent with a widely accepted view that RO membranes have a dense (non-porous) skin layer. Since the membrane is considered as a black box, the irreversible thermodynamics model does not take into account any intrinsic properties (e.g. dimension and hydrophobicity) of the solute. As a result, filtration experiments are required for each individual solute to determine

63 their permeability and separation co-efficient at several permeate flux values prior to any
64 simulation. In other words, the irreversible thermodynamics model can only be used when
65 existing experimental data are already available.

66 Unlike the irreversible thermodynamics model, the pore-flow model assumes that the
67 membrane skin layer has cylindrical (capillary) pores. Physicochemical properties of both the
68 membrane and the solute are considered in the pore-flow model. Thus, once the pore-flow
69 model has been calibrated with a reference solute, it can be used to simulate the rejection of
70 any other solutes without any additional experiments. The pore-flow model has been applied
71 mostly to nanofiltration (NF) membranes.[16–19] Bowen et al.[16] successfully applied the pore-
72 flow model to simulate the permeation of glycerol and glucose through NF membranes by
73 approximating their molecular shapes to be spherical. Kiso et al.[17] developed a more precise
74 model to predict the permeation of 24 alcohols through NF membranes by employing a non-
75 spherical molecular model. They reported that molecular width of these alcohols was the key
76 parameter for simulating their rejections.

77 Although being very useful, applications of the pore-flow model to RO membranes have only
78 been reported in a few recent studies. This is because of the conventional view that RO
79 membranes do not have pores. However, evidence of free-volume hole-size (or pores) in the
80 skin layer of RO membranes has recently been revealed using state-of-the-art positron
81 annihilation lifetime spectroscopy (PALS) analysis.[20] Thus, it is possible to justify the
82 application of the pore-flow model to RO membranes when the solute size is comparable to
83 the membrane free-volume hole-size. For example, using the pore-flow model, Kiso et al.[21,22]
84 recently demonstrated the precise prediction of the permeation of 24 alcohols and crown ethers
85 through RO membranes. In another recent study, Madsen et al.[23] successfully applied the pore-
86 flow model to simulate the permeation of pesticides through NF and RO membranes. However,
87 previous studies[21–23] were validated at a single permeate flux. In practice, the local (specific)

88 permeate flux varies considerably throughout the membrane vessel. Thus, it is essential to take
89 into account the effect of permeate flux on rejection so that the model can be applied to a full-
90 scale plant.

91 There have been no previous attempts to assess the application of the steric pore-flow
92 modelling approach for predicting the rejection of small and neutral TrOCs that are of great
93 concern in potable water reuse. The analysis of these TrOCs at the environment concentration
94 levels (part-per-million to part-per-trillion) requires sophisticated instrumentation (e.g. gas
95 chromatograph coupled with tandem mass spectrometer[24,25]) which is not always readily
96 available in a typical laboratory. Thus, the ability to estimate the rejection of many TrOCs by
97 RO membranes using the free-volume hole-size of an RO membrane determined by a single
98 solute can lead to a significant reduction in the cost associated with TrOCs analysis.

99 This study aimed to develop a new approach to apply the steric pore-flow model is developed
100 to predict the permeation of eight *N*-nitrosamines and seven VOCs that are of great concern in
101 potable water reuse through an RO membrane by estimating the free-volume hole-size with a
102 single reference solute. Free-volume hole-radius was estimated by pure water permeability and
103 experimentally measuring NDMA – as the only reference solute – at a specific permeate flux.
104 The predicted rejections of *N*-nitrosamines and VOCs were validated with their experimentally
105 obtained rejections attained under a range of permeate flux. The model was also integrated with
106 a membrane free-volume hole-radius previously obtained by PALS analysis and its accuracy
107 was compared with the model developed with a reference solute during the model validation
108 phase.

2. Modeling approach and theory

2.1 Procedure of model prediction

This study is based on the previous work by Kiso et al.[21,22] to predict the permeation of small and uncharged TrOCs through RO membranes. Parameters used in the model include molecular dimensions of TrOCs, free-volume hole-radius, free-volume hole-length and porosity of the membrane, and operating conditions (i.e. permeate flux and feed temperature). The membrane structural parameters can be determined by 1) physical methods such as microscopic techniques or 2) methods based on permeation and removal performance using reference solutes. In this study, the free-volume hole-length measured using scanning electron microscopy (SEM)[26] was used for model calculation. The free-volume hole-radius estimated using a single reference solute or analytically measured by PALS[20] was used for model calculation. The membrane porosity was estimated using the pure water permeability because there is no available physical method to measure membrane porosity. The calculation methodology is schematically described in **Fig. 1**.

The parameters except for the membrane porosity and the free-volume hole-radius (i.e. molecular radius, operating conditions and free-volume hole-length) were input to the predictive model **(Step 1 in Fig. 1)**. The pure water permeability of an RO membrane was measured to express the membrane porosity as a function of free-volume hole-radius **(Step 2 in Fig. 1)**. The membrane porosity was calculated in response to the input value of free-volume hole-radius. The free-volume hole-radius of an RO membrane was determined using NDMA as the reference solute. NDMA rejection by an RO membrane (ESPA2, Hydranautics/Nitto) was obtained at the standard permeate flux of 20 L/m^{2}h and feed solution temperature of 20 °C using a laboratory-scale filtration system **(Step 3 in Fig. 1)**. The free-volume hole-radius of the RO membrane was estimated by minimizing the variance between the experimentally obtained

and calculated NDMA rejection values **(Step 4 in Fig. 1)**. The estimated free-volume hole-radius was compared with the value previously determined by PALS analysis[20] **(Step 5 in Fig. 1)**. The estimated or analytically determined free-volume hole-radius as well as the membrane porosity calculated in response to these fee-volume hole-radius were used to predict the rejection of all TrOCs under a range of permeate flux **(Step 6 in Fig. 1)**. Finally, the predicted rejections of TrOCs in the model were validated by comparing with experimentally obtained values **(Step 7 in Fig. 1)**.

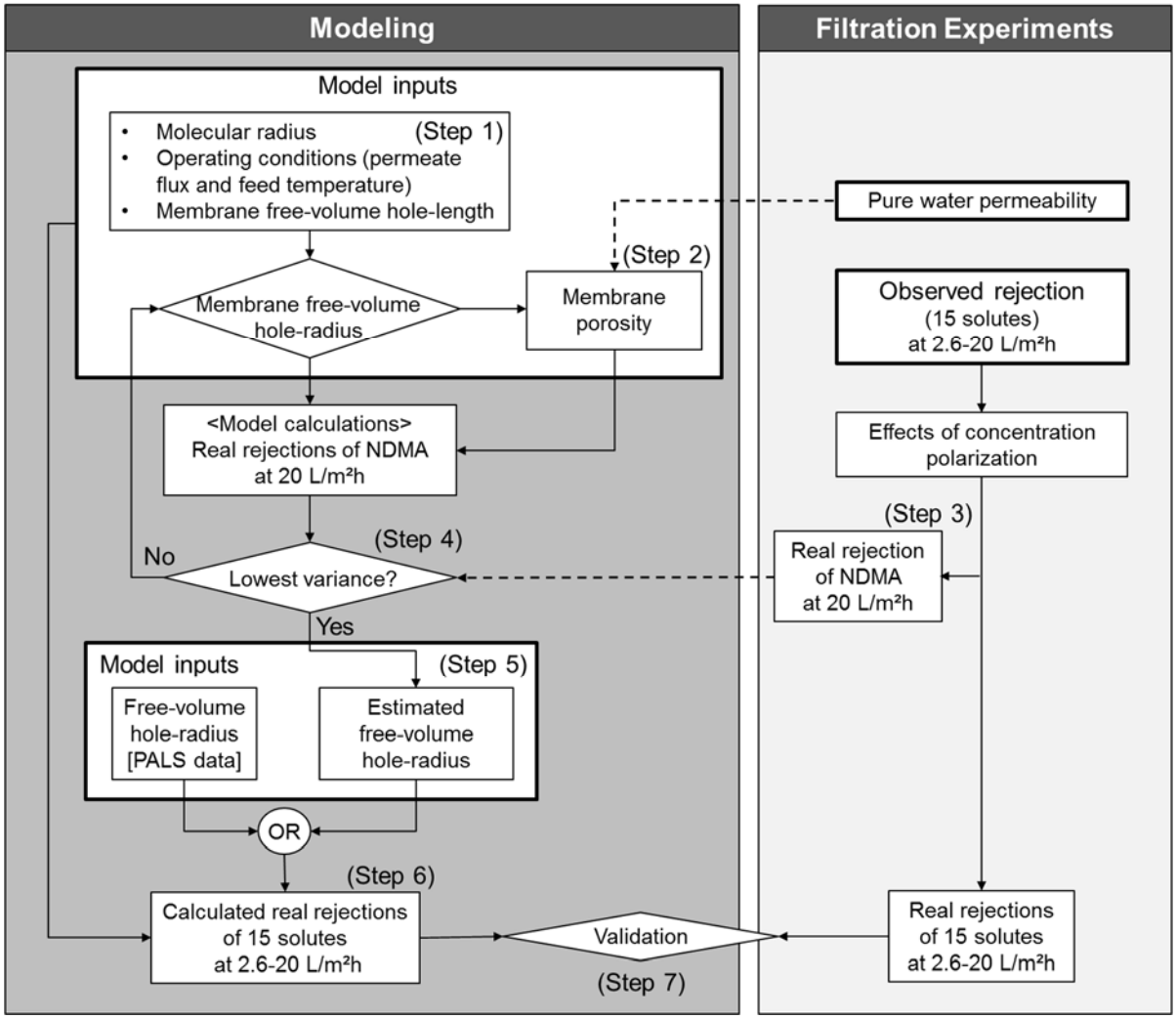

Fig. 1. Procedure of the model calculation.

2.2 Molecular geometric parameter

An organic molecule can be represented as a sphere, a parallelepiped, a cylinder or a disk shape.

When a parallelepiped is considered, molecular width (MW_d) and length (L) are used to present the geometric parameters for modeling. Molecular width is calculated as a half-length of the square root of area of rectangle enclosing the molecule perpendicular to the length axis of the molecule. When a cylindrical shape or disk shape is considered, molecular radius (r_c) and length (L) are used as the geometric parameters for modeling. Kiso et al.[21] reported that the parallelepiped approach (i.e. molecular width as the geometric parameter) provided a better fit for the rejection of alcohols while the disk-shaped approach (i.e. molecular radius as the geometric parameter) provided a better fit for the rejection of crown ethers.[22] Madsen et al.[23] reported that the parallelepiped approach resulted in a best fit for the rejection of pesticides by NF membranes while the cylindrical approach provided a better fit for RO membranes.

In this study, the molecular shape is approximated to be a cylinder for simplicity for calculating the rejection of *N*-nitrosamines and VOCs. The molecular radius was defined as a radius of the minimally projected graphic of a conformer (**Supplementary information Fig. S1**) base on a previous study by Fujioka et al.,[27] in which a strong correlation between the rejection of solutes and their minimum projection area was demonstrated. Results from the previous study indicates the minimally projected geometry of a conformer governs the solute rejection. The molecular length was defined as maximum extension of the conformer perpendicular to the minimally projected plane. The molecular geometry was calculated with Marvin Sketch (ChemAxon, Budapest, Hungary).

2.3 Steric pore-flow model

In the steric pore-flow model, solute permeation through the membrane is governed by the molecular sieving effect. In other words, a high solute permeation can be expected for a small molecule. A detailed description of the model is provided elsewhere[21,22,28] and a brief

explanation is given below.

The model describes solute permeation through an RO membrane with diffusive and convective transports through a hypothetical cylindrical capillary free-volume hole, where the tortuosity and the rugose morphology of polyamide RO membranes are ignored:

$$J_{s,pore} = -D_p \frac{dC}{dx} + J_{v,pore} K_c C \quad (1)$$

$$J_{s,pore} = J_{v,pore} C_p \quad (2)$$

where $J_{s,pore}$ and $J_{v,pore}$ are the solute and water flux in a free-volume hole; D_p ($D_p = K_d D_\infty$) and D_∞ are the diffusion coefficient of the solute in the free-volume hole and water, respectively; K_d and K_c are the solute hindrance factors for diffusion and convection, respectively; C is the solute concentration at axial position *x* within the free-volume hole; and C_p is the solute concentration of the bulk permeate.

In the steric pore-flow model, the water flux in a single free-volume hole is expressed by the Hagen-Poiseuille equation. The water flux in a single free-volume hole ($J_{v,pore}$) is equal to the permeate rate per unit surface area (J_v) divided by the membrane porosity as follows:

$$J_{v,pore} = \frac{J_v}{\varepsilon} = \frac{{r_p}^2(\Delta P - \Delta\pi)}{8\eta\Delta x} \quad (3)$$

where ε is the membrane porosity, r_p is the free-volume hole-radius, ΔP and $\Delta\pi$ are the applied pressure and the osmotic pressure, η is the viscosity of water, and Δx is the free-volume hole-length. Since the steric pore-flow model is based on the assumption that free-volume holes of RO membranes are cylindrical capillary pore,[16] the tortuosity of the membrane is not included in this model. The solvent viscosity in a pore (η) is calculated with the viscosity in the bulk (η_0) using the following equation suggested by Bowen et al.:[16]

$$\frac{\eta}{\eta_0} = 1 + 18\left(\frac{d}{r_p}\right) - 9\left(\frac{d}{r_p}\right)^2 \quad (4)$$

where d is solvent molecular diameter (0.28 nm for water). The viscosity in a pore influences water flux and solute diffusivity, but not solute rejection. The solvent viscosity in a pore was used for calculating water flux and solute diffusivity.

Solute rejection is obtained by integrating Eq. (1) across the membrane with the following boundary conditions:

$$c(x = 0) = \ c_m = \Phi C_m \quad (5)$$

$$c(x = \Delta x) = \ c_p = \Phi C_p \quad (6)$$

where c_m and c_p are the solute concentration in the membrane matrix at the feed and permeate side, respectively. C_m and C_p are the solute concentration at the membrane surface (outside of the membrane) and permeate in the bulk, respectively.

The integration yields the following formula for uncharged solute real rejection (R_{cal}):

$$R_{cal} = 1 - \frac{C_p}{C_m} = 1 - \frac{\Phi K_c}{1-[1-\Phi K_c]exp(-P_e)} \quad (7)$$

where Φ is a steric partition coefficient and P_e is the Peclet number. The Peclet number is defined as follows:

$$P_e = \frac{K_c J_{v,pore} \Delta x}{D_p} = \frac{K_c J_v \Delta x}{D_p \varepsilon} \quad (8)$$

In this model, solute rejection is independent of solute concentration in the RO feed. Although the rejection of inorganic salts can be affected by their concentrations in the feed due to electrostatic interactions,[29,30] the rejection of small and uncharged solutes by RO membranes at low concentration (ng/L to μg/L) is independent from their feed concentrations.[31–33]

Eqs. (7) and (8) indicate that uncharged solute rejections is characterized by permeate flux (J_v), the membrane structural parameters: the ratio of the length of the free-volume hole (Δx) and the membrane porosity (ε), and four model parameters: the solute hindrance factors (K_d and K_c), the solute diffusivity (D_p), and the steric partition coefficient (Φ). The four model parameters are determined from the ratio of molecular size to free-volume hole-radius, and feed water temperature.

The membrane porosity, for which measurement with physical methods is not available, is calculated with a semi-empirical method. By using Hagen-Poiseuille equation (Eq. (3)), the membrane porosity is expressed as the following equation:

$$\varepsilon = \left(\frac{8\eta \Delta x J_v}{\Delta P}\right)\frac{1}{{r_p}^2} \quad (9)$$

By substitution Eq. (9) into Eq. (8), Peclet number (P_e) can be calculated using applied pressure (ΔP) and free-volume hole-radius (r_p):

$$P_e = \frac{K_c J_v}{D_p}\frac{\Delta x}{\varepsilon} = \frac{K_c}{D_p}\frac{\Delta P {r_p}^2}{8\eta} \quad (10)$$

Eq. (10) suggests that the Peclet number is independent of the thickness of the membrane skin layer. Diffusivities in aqueous solution (D_∞) and in a free-volume hole (D_p) are calculated with the following equations:

$$D_\infty = \frac{KT}{6\pi\eta} \times \frac{1}{r_s} \quad (11)$$

$$D_p = K_d D_\infty \quad (12)$$

where K is the Boltzmann constant, T is absolute temperature and r_s is the Stokes radius. The Stokes radius (r_s) is calculated from solute radius (r_c) using the following correlation:

$$(r_s \times 10^{-9}) = 1.969 \times (r_c \times 10^{-9}) - 0.248 \quad (13)$$

The correlation was obtained by calculating the molecular radius of the compounds for which the Stokes radius was given by Kiso et al.,[35] and fitting them against the values of the Stokes radius. The correlation was used to calculate the Stokes radius of target compounds in the present study from their molecular radius.

The hindrance factors (K_d and K_c) are function of the ratio (λ) of the solute radius to the free-volume hole-radius, and expressed using the enhanced drag coefficient (K^{-1}) and the lag coefficient (G):

$$K_d = K^{-1}(\lambda) \quad (14)$$

$$K_c = (2 - \Phi)G(\lambda) \quad (15)$$

The hydrodynamic coefficients for the range of $0 < \lambda < 0.95$ are expressed as follows:[34]

$$K^{-1}(\lambda) = 1.0 - 2.30\lambda + 1.154\lambda^2 + 0.224\lambda^3 \quad (16)$$

$$G(\lambda) = 1.0 + 0.054\lambda - 0.988\lambda^2 + 0.441\lambda^3 \quad (17)$$

The same equations can be used for compounds with $\lambda > 0.95$, because their real rejections are very high and the impact of difference in λ on rejection prediction is negligible.

In the steric pore-flow model, the steric partition coefficient (Φ) is calculated by modeling the molecules by freely rotating parallelepipeds or cylinders.[21,23] In this study, the partition coefficient was calculated without rotating molecules for simplicity, and calculated by directing the basal plane of the cylindrical shape to the membrane surface. The partition coefficient (Φ) of a solute is calculated with the following equation:

$$\Phi = (1 - \lambda)^2 \quad (18)$$

2.4 Concentration polarization

Due to concentration polarization, the concentration of solutes at the vicinity of the membrane surface becomes greater than that in the bulk feed solution, and real rejection needs to be calculated with the concentration of solute in the permeate and at the vicinity of the membrane surface in the feed. In contrast, observed rejection is calculated with measurable concentrations – solute concentrations in the permeate and bulk feed solution. In this study, the real rejection (R_{real}) is calculated from the observed rejection (R_{obs}) by using the following equation:[36]

$$R_{real} = \frac{R_{obs}\exp(J_v/k)}{1+R_{obs}[exp(J_v/k)-1]} \quad (19)$$

where k is mass transfer coefficient determined by Sherwood number (S_h). The Sherwood number was calculated using the following formula that is applicable for incomplete solute rejections ($0.75 < R_{real} < 1$):[37]

$$S_h = \frac{d_h k}{D_\infty} = 1.195 Re^{0.554} Sc^{0.371} \left(\frac{d_h}{L_m}\right)^{0.131} \quad (20)$$

where S_h is the Sherwood number, d_h is the hydraulic diameter of the flow channel, Re is the Reynolds number, Sc is the Schmidt number and L_m is the length of membrane. The solute diffusivity in aqueous solution (D_∞) is calculated using Eq. (14) with the viscosity in the bulk. The hydraulic diameter and flow velocity in the feed channel are calculated with the following equation:

$$d_h = \frac{ab}{a+2b} \quad (21)$$

$$v = \frac{Q_r}{ab} \quad (22)$$

where a and b are cell width and height, respectively, and Q_r is the retentate flow rate. The

values of these parameters a, b, L_m and Q_r used in this study were 0.04 m, 0.002 m, 0.18 m and 1.67×10^{-5} m^3/s, respectively.

3. Materials and method

3.1 Chemicals

Eight *N*-nitrosamines and fifteen VOCs were selected in this study **(Table 1)**. All *N*-nitrosamines were of analytical grade and purchased from Supelco (Bellefonte, PA, USA). A stock solution was prepared in pure methanol (Wako Pure Chemical Industries, Tokyo, Japan) at 1 mg/L of each *N*-nitrosamine. A cocktail of VOCs (1 mg/ml of each VOC in methanol) was obtained from Kanto Chemical (Tokyo, Japan). Eight deuterated *N*-nitrosamines, *N*-nitrosodimethylamine-d6 (NDMA-d6), *N*-nitrosomethylethylamine-d3 (NMEA-d3), *N*-nitrosopyrrolidine-d8 (NPYR-d8), *N*-nitrosodiethylamine-d10 (NDEA-d10), *N*-nitrosopiperidine-d10 (NPIP-d10), *N*-nitrosomorpholine-d8 (NMOR-d8), *N*-nitrosodipropylamine-d14 (NDPA-d14) and *N*-nitrosodi-n-butylamine-d18 (NDBA-d18) were also used as surrogate. These deuterated chemicals were obtained from CDN isotopes (Pointe-Claire, Quebec, Canada). A stock solution was prepared in pure methanol at 1 mg/L of each deuterated *N*-nitrosamine. Dichloroacetonitrile (1 mg/ml in methanol) was supplied by Wako Pure Chemical Industry. Deuterated 1,4-dioxane (1,4-dioxane-d8) (2 mg/ml in methanol) was purchased from Wako Pure Chemical Industries and was used as surrogate for VOCs analysis. Deuterated toluene (toluene-d8) and fluorobenzen were purchased from Supelco and were used as internal standard. All stock solutions were stored at -20 °C in the dark. NaH_2PO_4 and Na_2HPO_4 used for pH adjustment, and pure sodium hydroxide used for GC-MS analysis were supplied from Wako Pure Chemical Industries.

Table 1 Properties of selected compounds.

Compound	Molecular weight [a] [g/mol]	Log *D* at pH 7 [a]	pKa [a]	Henry's law constant at 25 °C [atm,m^3/mol]	Minimum projection area [a] [Å^2]	Molecular radius [nm]	Molecular length [a] [nm]	Diffusion coefficient at 20 °C [nm^2/s]
NDMA	74.08	0.08	3.22	1.20×10^{-6} [b]	19.40	0.248	0.683	8.88×10^{8}
NMEA	88.11	0.41	3.42	1.44×10^{-6} [b]	22.03	0.265	0.771	7.84×10^{8}
NPYR	100.12	0.39	3.30	1.99×10^{-7} [b]	25.04	0.282	0.773	6.96×10^{8}
NDEA	102.14	0.75	3.32	1.73×10^{-6} [b]	24.24	0.278	0.903	7.17×10^{8}
NPIP	114.15	0.81	3.30	2.81×10^{-7} [b]	28.64	0.302	0.812	6.18×10^{8}
NMOR	116.12	-0.32	3.14	2.13×10^{-10} [b]	26.92	0.293	0.665	6.53×10^{8}
NDPA	130.19	1.05	3.30	3.46×10^{-6} [b]	27.37	0.295	1.157	6.43×10^{8}
NDBA	158.25	2.56	3.30	9.96×10^{-6} [b]	28.62	0.302	1.405	6.19×10^{8}
1,1,1-Trichloroethane	133.40	2.08	N.I.	1.72×10^{-2} [c]	25.46	0.285	0.635	6.86×10^{8}
1,1,2-trichloroethane	133.40	2.17	N.I.	9.12×10^{-4} [c]	22.39	0.267	0.752	7.72×10^{8}
1,1-Dichloroethane	98.95	1.52	N.I.	5.61×10^{-3} [c]	20.86	0.258	0.627	8.26×10^{8}
1,2-Dichloropropane	112.98	1.92	N.I.	2.80×10^{-3} [c]	22.64	0.268	0.1.97	7.64×10^{8}
1,4-Dichlorobenzene	147.00	3.18	N.I.	2.43×10^{-3} [c]	20.38	0.255	0.964	8.45×10^{8}
Benzen	78.11	1.97	N.I.	5.56×10^{-3} [c]	18.70	0.244	0.724	9.22×10^{8}
Bromodichloromethane	163.82	1.98	N.I.	1.63×10^{-3} [c]	20.85	0.258	0.656	8.27×10^{8}
Bromoform	252.73	2.28	N.I.	5.34×10^{-4} [c]	22.64	0.268	0.683	7.64×10^{8}
Carbontetrachloride	153.81	3.00	N.I.	N.A.	25.00	0.282	0.631	6.97×10^{8}
Chloroform	119.37	1.83	N.I.	5.56×10^{-3} [c]	19.95	0.252	0.636	8.63×10^{8}
Dibromochloromethane	208.28	2.13	N.I.	7.83×10^{-4} [c]	21.50	0.262	0.681	8.02×10^{8}
Dichloroacetonitrile	109.94	1.12	N.I.	3.79×10^{-6} [d]	21.23	0.260	0.679	8.12×10^{8}
Tetrachloroethane	167.84	2.41	N.I.	N.A.	26.61	0.291	0.763	6.59×10^{8}
Toluene	92.14	2.49	N.I.	6.63×10^{-3} [c]	20.88	0.258	0.821	8.25×10^{8}
Trichloroethene	131.38	2.18	N.I.	N.A.	18.58	0.243	0.719	9.28×10^{8}

[a] Calculated with Marvin Sketch;

[b] [8];

[c] US EPA, https://www3.epa.gov/ceampubl/learn2model/part-two/onsite/esthenry.html;

[d] US NLM, https://chem.nlm.nih.gov/chemidplus/rn/3018-12-0;

N.I.: non-ionized, N.A.: not available.

3.2 RO membrane properties

A thin-film composite polyamide RO membrane (ESPA2, Hydranautics/Nitto) was used. The

ESPA2 membrane has an ultrathin polyamide active skin layer on a porous supporting layer. The ESPA2 membrane has an active skin layer thickness of 20 nm according to a previous study using scanning electron microscopy (SEM).[26] We have previously characterized the mean free-volume hole-radius of 0.289 nm within the active skin layer of the ESPA2 membrane.[20]

3.3 Experimental protocol

The RO membrane treatment system consisted of a 2 L feed tank, a feed pump (FTU-1, Membrane Solution Technology, Shiga, Japan), and an acrylic membrane cell (C-10T, Nitto, Osaka, Japan) with an effective membrane area of 60 cm^2 **(Supplementary information Fig. S3)**. All membrane samples were rinsed with Milli-Q water. The membrane was then compacted using Milli-Q water at 0.7 MPa for 2 h. Once permeate flux was stabilized, pure water permeability of the membrane was measured at the feed pressure of 0.7 MPa. Feed solution temperature was maintained at 20 °C throughout the experiments. After the measurement of pure water permeability, phosphate buffer was introduced to the feed tank to adjust the solution pH to 7. A stock solution of *N*-nitrosamines was added to the feed tank to obtain 2 μg/L of each *N*-nitrosamine. Each VOC was added to the feed tank to obtain 100 μg/L of each VOC.

The filtration system was operated in a recirculation mode at a cross-flow velocity of 0.21 m/s. Both permeate and concentrate were circulated back to the feed tank throughout the experiments. Before the first sampling event, the feed was recirculated for 1 h to achieve the steady state conditions in *N*-nitrosamine rejection, and for 24 h to minimize the adsorption of VOCs on the membrane surface. The effects of permeate flux on solute rejections were evaluated by incrementally reducing the permeate flux from 20 to 2.6 L/m^2h. Before each sampling event, the system was operated at a fixed permeate flux for at least 30 min to attain the stable separation of target compounds. From the feed and permeate streams, two samples

(50 mL and 40 mL) were collected for the analysis of *N*-nitrosamines and VOCs, respectively. Since the permeate flow decreased from 2 to 0.26 mL/min as the permeate flux was reduced from 20 to 2.6 L/m^{2}h, the sampling period increased from 20 min to 150 min to collect 40 mL of permeate samples for VOCs analysis. The observed rejection (R_{obs}) was calculated by the following equation:

$$R_{obs} = 1 - \frac{C_p}{C_f} \quad (22)$$

where C_p and C_f are the concentrations in the permeate and the feed, respectively.

3.4 Analytical techniques

3.4.1 *N*-nitrosamines

N-nitrosamines concentrations were determined using a previously developed analytical method[24] that involves solid phase extraction (SPE) and analytical quantification using gas chromatograph (GC) coupled with tandem mass spectrometer (MS/MS). Prior to the SPE step, surrogate stock solution was spiked into each sample at 20 ng of each surrogate. *N*-nitrosamines were then extracted using Sep-Pak NH-2 and AC-2 cartridges (Waters, MA, USA) at a flow rate of 10 mL/min. After drying the AC-2 cartridges, the analytes from the cartridges were eluded using 2 mL dichloromethane (Wako Pure Chemical Industries, Tokyo, Japan). The eluents were concentrated under the nitrogen gas stream. After the resulting eluent was added with 50 µL of the dichloromethane solution and 25 µL of the toluene-d8 stock solution (1 mg/L in dichloromethane), *N*-nitrosamine concentration was quantified using Varian 450 series GC coupled with a Varian 300 series MS/MS. Triplicate analysis was conducted for each sample to calculate their mean concentrations, which were used for the calculation of experimentally obtained rejection.

346 3.4.2 Volatile organic compounds

347 Concentrations of VOCs were determined by headspace solid phase microextraction-gas
348 chromatography-mass spectrometry (SPME-GC-MS).[25] A 100 μm PDMS fiber (Supelco,
349 Bellefonte, PA, USA) was selected for extraction because the fiber provides a wide range of
350 linearity for VOCs in multiple-component system.[25] The fiber was thermally conditioned at
351 250 °C for 30 min. Three grams of sodium chloride was added to a 20 mL glass vial, which
352 was followed by the addition of 10 mL of samples and a surrogate solution containing 1,4-
353 dioxane-d8 (100 μg/L) into the vial. A PTFE-faced septum cap was immediately crimped on
354 the vial. After sodium chloride was dissolved, the fiber was exposed in the headspace of the
355 sample for 30 min at 60 °C. Finally, the fiber was removed from the vial and immediately
356 inserted into a GC injection port for thermal desorption of the extracted analytes for 4 min.
357 Only samples with 1,4-dioxane- d_8 recovery of over 50% were considered valid.

358 # 4. Results and discussion

359 ## 4.1 Stability of *N*-nitrosamines and VOCs

360 Most *N*-nitrosamines selected in this study can be classified as hydrophilic (Log $D \leq 2$) and
361 non-volatile compounds (Henry's law constant $\leq 1\times10^{-5}$), thus, their hydrophobic interaction
362 with the membrane is expected to be negligible.[38–40] These *N*-nitrosamines are stable in the
363 aqueous phase; thus, they do not adsorb to the solid phase or evaporate. By contrast, some
364 VOCs are more hydrophobic (e.g. Log $D \geq 2$) and more volatile than *N*-nitrosamines,
365 indicating that the adsorption of these hydrophobic VOCs onto the RO membrane and their
366 volatilization could occur.[40] In fact, the concentrations of most VOCs in the feed continuously
367 decreased over 19 h of the system operation **(Supplementary information Fig. S4)**. As a result,
368 this study used the data of only seven VOCs (chloroform, bromodichloromethane,
369 dichloroacetonitrile, dibromochloromethane, 1,1,2-trichloroethane, 1,2-dichloropropane and

370 bromoform) that remained over 50% of their initial concentrations in the feed after 19 h of
371 filtration operation.

372 **4.2 Experimentally obtained rejection of *N*-nitrosamines and VOCs**

373 Real rejections by ESPA2 membrane were calculated with their observed rejections. The real
374 rejection of *N*-nitrosamines at the permeate flux of 20 L/m^{2}h was 56% for NDMA, 84% for
375 NMEA, 89% for NPYR and >96% for the five remaining *N*-nitrosamines (i.e. NDEA, NPIP,
376 NMOR, NDPA and NDBA) **(Fig. 2)**. Real rejections of the seven VOCs by ESPA2 membrane
377 at the permeate flux of 20 L/m^{2}h were 54% for chloroform, 69% for bromodichloromethane,
378 84% for dichloroacetonitrile, 83% for dibromochloromethane, 85% for 1,1,2-trichloroethane,
379 90% for 1,2-dichloropropane and 91% for bromoform **(Fig. 2)**. Since the analytical accuracy
380 of the seven VOCs under the permeate flux of 5 L/m^{2}h was low, the rejection data of the seven
381 VOCs at the permeate flux of 5 L/m^{2}h are not shown. Compound rejection by the RO
382 membrane increased in order of increasing molecular radius, with the notable exception of
383 NPYR. The results indicate that molecular radius can be a property that governs the permeation
384 of most *N*-nitrosamines and VOCs through the RO membrane. The observed and real rejection
385 of target compounds at each permeate flux is presented in **Supplementary information Table**
386 **S2**.

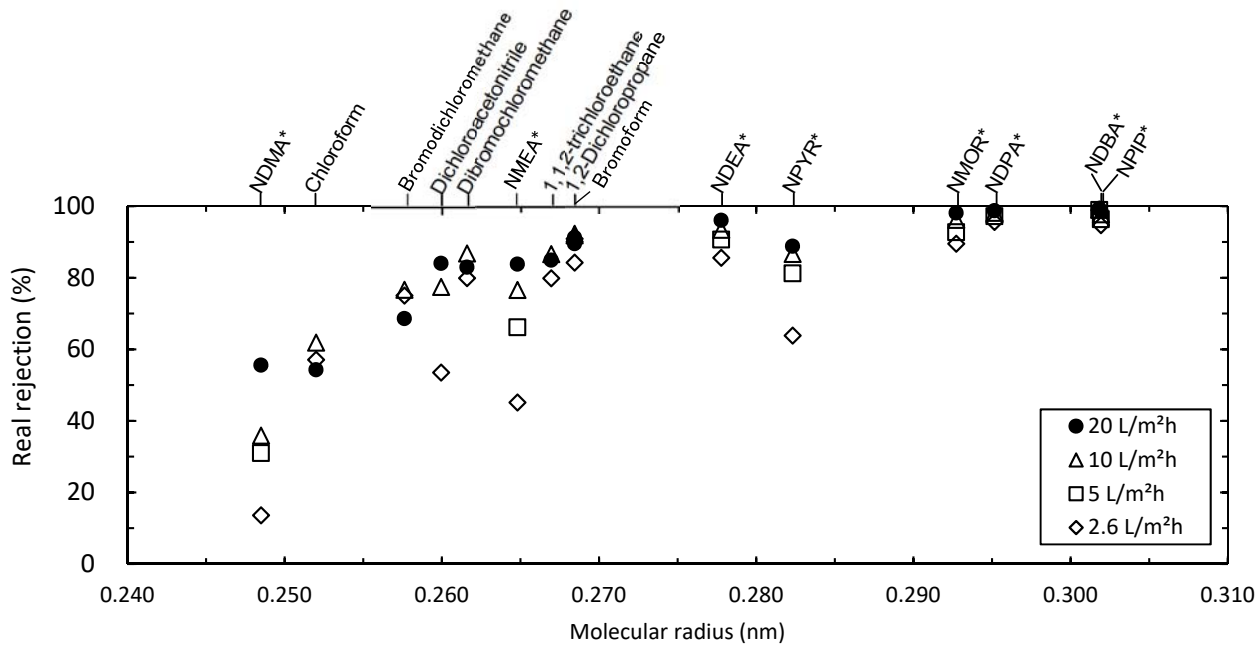

Fig. 2. Experimentally obtained real rejection of *N*-nitrosamines (*) and VOCs by the ESPA2 membrane as a function of their molecular radius (permeate flux = 2.6–20 L/m^{2}h, cross-flow velocity = 0.21 m/s, feed solution temperature = 20 °C and feed pH = 7). The rejection data of the seven VOCs at the permeate flux of 5 L/m^{2}h are not shown due to the low analytical accuracy.

N-nitrosamine rejection by ESPA2 membrane increased with increasing permeate flux **(Fig. 3a)**. The impact of permeate flux on *N*-nitrosamine rejection was more significant for compounds with short molecular radius. Increasing permeate flux from 2.6 to 20 L/m^{2}h resulted in an increase in NDMA, NMEA and NPYR rejection from 14 to 56%, from 45 to 84%, and from 64 to 89%, respectively. The impact of permeate flux on *N*-nitrosamine rejection was less significant for long molecular radius compounds (i.e. NDEA, NPIP, NMOR, NDPA and NDBA). The increase in *N*-nitrosamine rejection in response to an increase in permeate flux can be attributed to convective transport of water which proportionally increases according to transmembrane pressure increase, while diffusion transport of solutes remains almost constant with the increased transmembrane pressure.[41–43] In other words, as the permeate flux increases, water molecules passes through the RO membranes more progressively relative to *N*-

nitrosamines. This leads to a lower *N*-nitrosamine concentration in the RO permeate, which gives higher *N*-nitrosamine rejection. In contrast to *N*-nitrosamines, the rejection of some VOCs remained almost constant at the permeate flux of 2.6-20 L/m^{2}h **(Fig. 3b)**. The only exception was dichloroacetonitrile, which revealed a similar trend to *N*-nitrosamines.

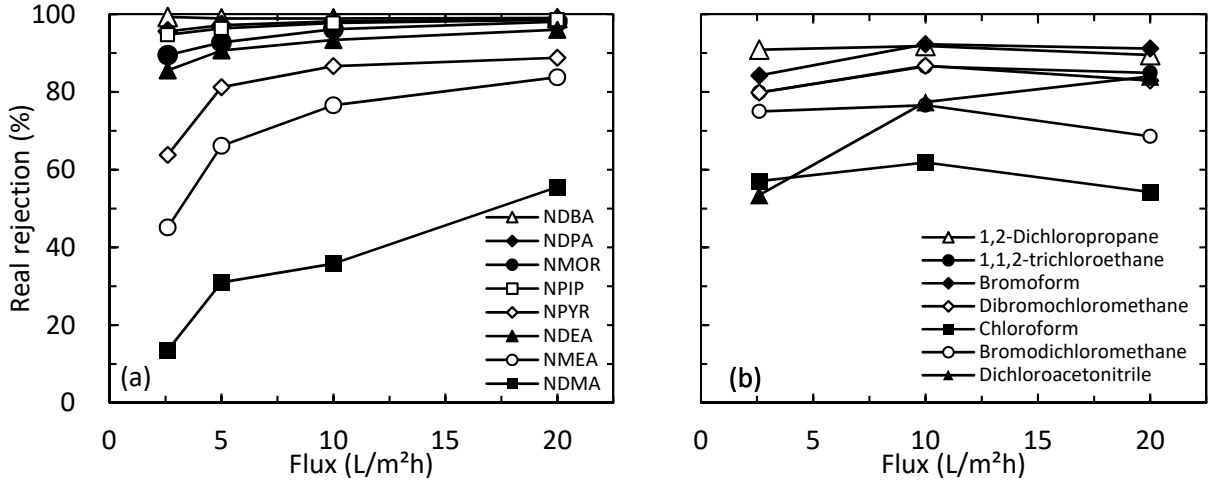

Fig. 3. Experimentally obtained rejection of (a) *N*-nitrosamines and (b) VOCs by the ESPA2 membrane as a function of permeate flux. Experimental conditions are described in Fig. 2.

4.3 Free-volume hole-radius estimation using NDMA

As described in **Fig. 1**, the membrane porosity is expressed as a function of free-volume hole-radius by using the pure water permeability. The experimentally obtained pure water permeability (66 L/m^{2}hMPa) was used for the calculation of membrane porosity, and then, the membrane porosity was calculated in response to the input value of free-volume hole-radius **(Step 2 in Fig. 1)**. The free-volume hole-radius of the ESPA2 membrane was estimated by minimizing the variance between the calculated real NDMA rejection and the experimentally obtained real rejection ($(R_{cal} - R_{real})^2$) under the condition of permeate flux of 20 L/m^{2}h **(Step 4 in Fig. 1)**. The minimization of variance was performed using a program Solver in software Excel, in which the minimum value of variance is calculated by changing the free-volume hole-radius. As a result, the free-volume hole-radius that showed the minimum

variance was identified at 0.348 nm. The calculated NDMA rejection as a function of the free-volume hole-radius and the variance between the calculated and the experimentally obtained NDMA rejections are presented in **Fig. 4**. The estimated free-volume hole-radius was larger than the free-volume hole-radius of 0.289 nm which was previously determined by PALS.[20] Using the values of the free-volume hole-radius, the membrane porosity was calculated to be 23.3% with the estimated free-volume hole-radius (0.348 nm), and 35.1% with the previously determined by PALS (0.289 nm). The membrane porosity as a function of the free-volume hole-radius is presented in **Fig. 4**. The calculated membrane porosities were used for model validation in the next section.

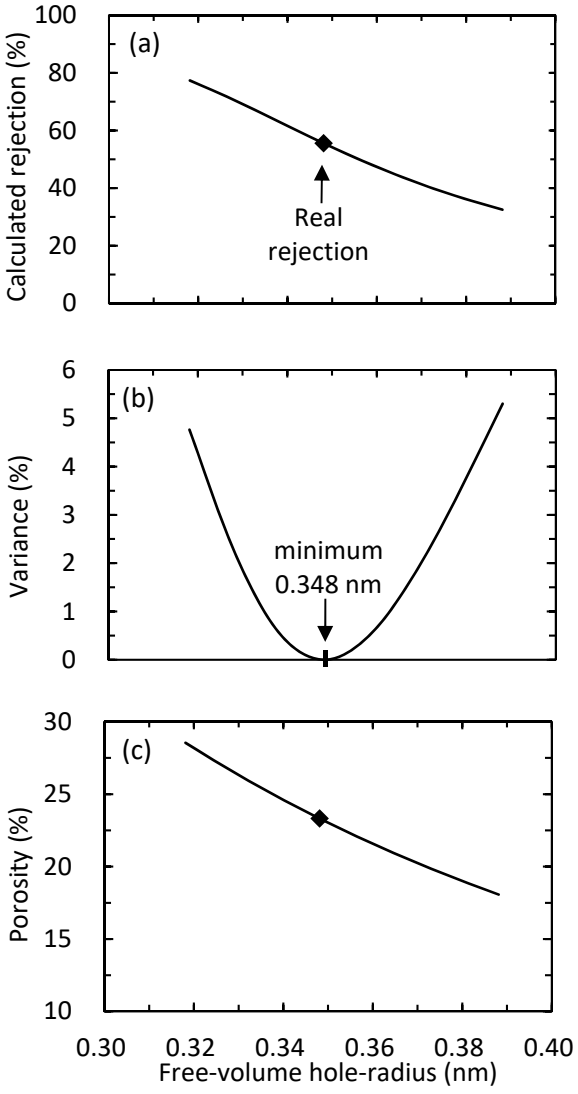

Fig. 4. (a) The calculated NDMA rejection as a function of the free-volume hole-radius, (b)

variance between the experimentally obtained and calculated NDMA rejections and (c) the calculated membrane porosity as a function of the free-volume hole-radius (permeate flux = 20 L/m^{2}h, feed solution temperature = 20 °C, free-volume hole-length = 20 nm and pure water permeability = 66 L/m^{2}hMPa).

4.4 Validation for *N*-nitrosamines

The model incorporated with the estimated free-volume hole-radius of 0.348 nm was validated under a range of permeate flux (2.6 to 20 L/m^{2}h) for predicting the rejection of *N*-nitrosamines. The predicted rejections of all eight *N*-nitrosamines **(Supplementary information Fig. S5a)** were in agreement with the experimentally obtained rejections ($R^2 = 0.97$) **(Fig. 5a)**. The strong correlation between the predicted and experimentally obtained rejections suggests that the model is capable of calculating the rejection of *N*-nitrosamines and only one model surrogate (i.e. NDMA) is sufficient for free-volume hole-radius estimation.

The model incorporated with the free-volume hole-radius determined by PALS (i.e. 0.289 nm[20]) was also validated. The predicted *N*-nitrosamine rejections under a range of permeate flux (2.6 to 20 L/m^{2}h) were higher than the experimentally obtained rejections **(Fig. 5b)**, resulting in an overestimation of *N*-nitrosamine rejections. Free-volume hole-radius determination by PALS is a particularly useful since no filtration experiments are required for model development. Nevertheless, results reported here indicate that additional adjustment is required to allow for more accurate prediction by the model using PALS data.

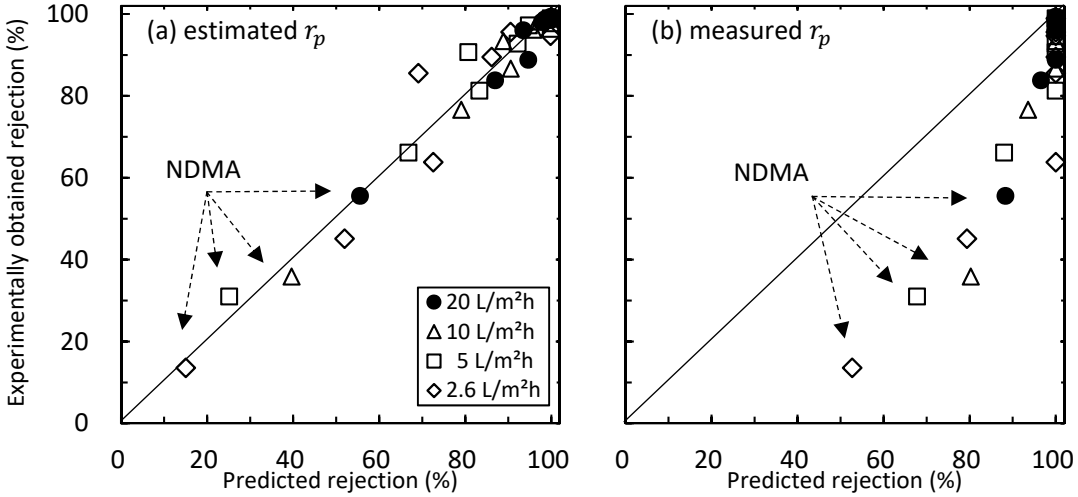

Fig. 5. Correlation between predicted and experimentally obtained real rejections of eight *N*-nitrosamines. The rejections were predicted by incorporating (a) estimated free-volume hole-radius (0.348 nm) and (b) free-volume hole-radius measured by PALS (0.289 nm) in the model (feed solution temperature = 20 °C and permeate flux = 2.6–20 L/m^{2}h).

4.5 Validation for VOCs

The model incorporated with the estimated free-volume hole-radius of 0.348 nm was also validated for VOCs. As a result, the model successfully predicted the rejection of VOCs at 20 L/m^{2}h permeate flux (R^2 = 0.98) **(Fig. 6a)**. However, the predicted rejections of VOCs except dichloroacetonitrile **(Supplementary information Fig. S5b)** were lower than their experimentally obtained rejections at the permeate flux of ≤10 L/m^{2}h **(Fig. 6a)**. The high experimentally obtained rejections may be due to the excessive volatilization of VOCs from the RO permeate during the prolonged samplings. The selected VOCs other than dichloroacetonitrile have relatively high Henry's law constant (>5.34×10^{-4}), thus, they are more volatile than dichloroacetonitrile and *N*-nitrosamines **(Table 1)**. As the permeate flux was reduced from 20 to 2.6 L/m^{2}h, the permeate flow decreased from 2 to 0.26 mL/min. Therefore, the sampling period increased from 20 min to 150 min to collect 40 mL of permeate samples for VOCs analysis. The prolonged sampling period at a low permeate flux causes more volatilization of VOCs from the RO permeate, leading to a lower VOC concentration in the RO

permeate. As a result, the lowered concentration in the RO permeate causes an overestimation of VOC rejections in rejection calculation. The correlation between Henry's law constant and the variance between the predicted and experimentally obtained real rejections of the VOCs was presented in **Supplementary information Fig. S6**. On the other hand, the predicted rejections of dichloroacetonitrile, which has a relatively low Henry's law constant, was in line with the experimentally obtained rejections under the permeate flux of 2.6–20 L/m^{2}h (R^2 = 0.95) **(Fig. 6b)**. To allow for more accurate prediction of VOC rejection, sampling techniques to avoid volatilization during filtration need to be reviewed in a future study.

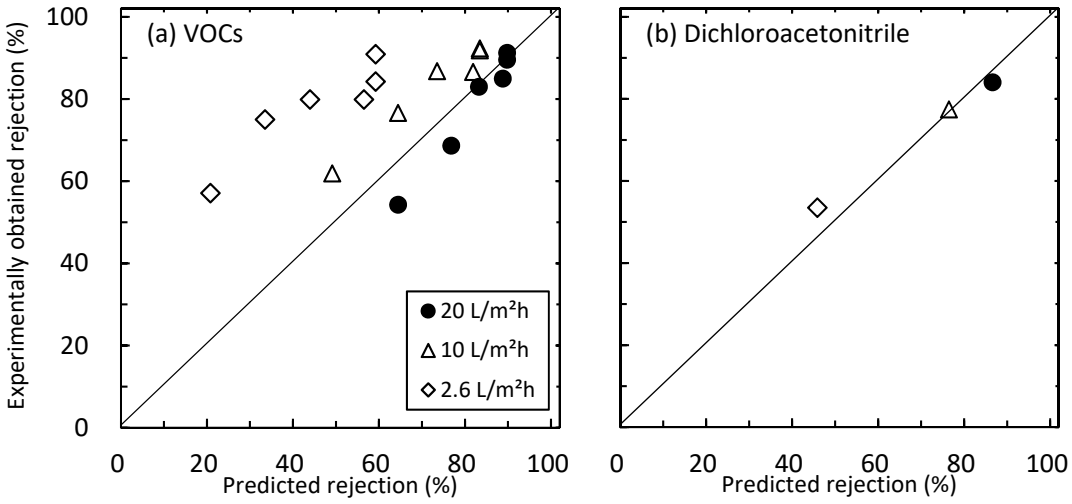

Fig. 6. Correlation between predicted and experimentally obtained rejections of (a) six VOCs and (b) dichloroacetonitrile (feed solution temperature = 20°C and permeate flux = 2.6–20 L/m^{2}h). The rejections were predicted by incorporating the estimated free-volume hole-radius (0.348 nm).

5 Conclusions

In this study, we proposed a new approach to apply the steric pore-flow model to predict the rejection of eight *N*-nitrosamines and seven VOCs that are of great concern in potable water reuse through an RO membrane. Using our approach, solute rejection is predicted by estimating the free-volume hole-size with a single reference solute and membrane pure water permeability.

This approach can lead to a significant reduction in labour and its associated cost for the evaluation of TrOCs removal by RO membranes. The key geometric parameter of membrane in this model was free-volume hole-radius, which was obtained from the experimentally obtained rejection of a reference solute (NDMA). The estimated free-volume hole-radius (0.348 nm) was larger than the free-volume hole-radius determined previously by PALS analysis (0.289 nm). The model incorporated with the estimated free-volume hole-radius could accurately predict the rejection of *N*-nitrosamines under a range of permeate flux. The model could accurately predict the rejection of seven VOCs at 20 L/m^{2}h permeate flux, but overestimated at ≤10 L/m^{2}h permeate flux due possibly to the excessive volatilization of these VOCs during the prolonged sampling periods. Future investigation need to be focused on the minimization of their loss during filtration experiments including sampling collections. Among the VOCs, a less volatile compound – dichloroacetonitrile – was the only chemical whose rejection was well predicted under a range of permeate flux. The model was also validated using the membrane free-volume hole-radius value previously obtained from PALS analysis. Using PALS data resulted in some over-prediction. The results suggest that PALS analysis cannot allow for model prediction unless additional adjustment is provided to improve the prediction accuracy.

Nomenclature

List of symbols

A	membrane surface area (m^2)
a	cell width (m)
b	cell height (m)
C	solute concentration in a free-volume hole (mg/L)
C_f	feed concentration (mg/L)
C_m	solute concentration at a membrane surface (mg/L)
C_p	permeate feed concentration (mg/L)
c_m	solute concentration at inlet of a free-volume hole (mg/L)
c_p	solute concentration at outlet of a free-volume hole (mg/L)
D_∞	diffusion coefficient in bulk solution (m^2/s)

d_h	hydraulic diameter of a flow channel (m)
D_p	diffusion coefficient of a solute in a free-volume hole (m^2/s)
G	lag coefficient (−)
$J_{s,pore}$	solute flux in a free-volume hole (L/m^2h)
$J_{v,pore}$	water flux in a free-volume hole (L/m^2h)
J_v	water flux (L/m^2h)
K	Boltzmann constant (J/K)
k	mass transfer coefficient (m/s)
K^{-1}	enhanced drag coefficient (−)
K_c	solute hindrance factors for convection (−)
K_d	solute hindrance factors for diffusion (−)
L_m	length of membrane (m)
P_e	Peclet number (−)
ΔP	applied pressure (N/m)
Q	permeate flow (m^3/s)
Q_r	concentrate flow rate (m^3/s)
R_{cal}	calculated rejection (−)
Re	Reynolds number (−)
R_{obs}	observed rejection (−)
R_{real}	real rejection (−)
r_c	solute radius (m)
r_p	free-volume hole-radius (m)
r_s	Stokes radius (m)
S_h	Sherwood number (−)
S_c	Schmidt number (−)
T	temperature (°C)
v	flow velocity (m/s)

Δx	length of a free-volume hole (m)
Greek letters	
Φ	steric partition coefficient (−)
ε	membrane porosity (−)
η	solvent viscosity in a free-volume hole (mPa·s)
η_0	solvent viscosity in bulk (mPa·s)
λ	ratio of solute radius to free-volume hole-radius (−)

6 Conflicts of interest

There are no conflicts to declare.

7 Acknowledgements

The authors acknowledge Hydranautics/Nitto for providing RO membrane elements.

8 Reference

1 D. Gerrity, B. Pecson, R. Shane Trussell and R. Rhodes Trussell, *J. Water Supply Res. Technol. - AQUA*, 2013, **62**, 321–338.

2 J. E. Drewes, G. Amy, C. Bellona and G. Filteau, *Comparing nanofiltration and reverse osmosis for treating recycled water*, 2008, vol. 100.

3 A. A. Alturki, N. Tadkaew, J. A. McDonald, S. J. Khan, W. E. Price and L. D. Nghiem, *J. Memb. Sci.*, 2010, **365**, 206–215.

4 Y. Luo, W. Guo, H. H. Ngo, L. D. Nghiem, F. I. Hai, J. Zhang, S. Liang and X. C. Wang, *Sci. Total Environ.*, 2014, **473–474**, 619–641.

5 K. L. Linge, P. Blair, F. Busetti, C. Rodriguez and A. Heitz, *J. Water Supply Res. Technol. - AQUA*, 2012, **61**, 494–505.

6 E. Agus, L. Zhang and D. L. Sedlak, *Water Res.*, 2012, **46**, 5970–5980.

7 C. Bellona, J. E. Drewes, P. Xu and G. Amy, *Water Res.*, 2004, **38**, 2795–2809.

8 T. Fujioka, S. J. Khan, Y. Poussade, J. E. Drewes and L. D. Nghiem, *Sep. Purif. Technol.*, 2012, **98**, 503–515.

9 C. Rodriguez, K. Linge, P. Blair, F. Busetti, B. Devine, P. Van Buynder, P. Weinstein and A. Cook, *Water Res.*, 2012, **46**, 93–106.

10 H. N. Altalyan, B. Jones, J. Bradd, L. D. Nghiem and Y. M. Alyazichi, *J. Water Process Eng.*, 2016, **9**, 9–21.

11 M. H. Plumlee, M. López-Mesas, A. Heidlberger, K. P. Ishida and M. Reinhard, *Water Res.*, 2008, **42**, 347–355.

12 Y. Poussade, A. Roux, T. Walker and V. Zavlanos, *Water Sci. Technol.*, 2009, **60**, 2419–2424.

13 J. Wang, D. S. Dlamini, A. K. Mishra, M. T. M. Pendergast, M. C. Y. Wong, B. B. Mamba, V. Freger, A. R. D. Verliefde and E. M. V Hoek, *J. Memb. Sci.*, 2014, **454**, 516–537.

14 O. Kedem and A. Katchalsky, *Biochim. Biophys. Acta*, 1958, **27**, 229–246.

15 C. Bellona, K. Budgell, D. Ball, K. Spangler, J. Drewes and S. Chellam, *IDA J.*, 2011, **3**, 40–44.

16 W. R. Bowen and J. S. Welfoot, *Chem. Eng. Sci.*, 2002, **57**, 1121–1137.

17 Y. Kiso, K. Muroshige, T. Oguchi, T. Yamada, M. Hhirose, T. Ohara and T. Shintani, *J. Memb. Sci.*, 2010, **358**, 101–113.

18 L. D. Nghiem, A. I. Schäfer and M. Elimelech, *Environ. Sci. Technol.*, 2004, **38**, 1888–1896.

19 A. R. D. Verliefde, E. R. Cornelissen, S. G. J. Heijman, E. M. V Hoek, G. L. Amy, B. Van Der Bruggen and J. C. Van Dijk, *Environ. Sci. Technol.*, 2009, **43**, 2400–2406.

20 T. Fujioka, N. Oshima, R. Suzuki, W. E. Price and L. D. Nghiem, *J. Memb. Sci.*, 2015, 486, 106–118.

21 Y. Kiso, K. Muroshige, T. Oguchi, M. Hirose, T. Ohara and T. Shintani, *J. Memb. Sci.*, 2011, **369**, 290–298.

22 Y. Kiso, T. Oguchi, Y. Kamimoto, K. Makino, Y. Takeyoshi and T. Yamada, *Sep. Purif. Technol.*, 2017, **173**, 286–294.

23 H. T. Madsen and E. G. Søgaard, *Sep. Purif. Technol.*, 2014, **125**, 111–119.

24 S. Yoon, N. Nakada and H. Tanaka, *Water Sci. Technol.*, 2013, **68**, 2118–2126.

25 S. Nakamura and S. Daishima, *Anal. Chim. Acta*, 2005, **548**, 79–85.

26 H. Yan, X. Miao, J. Xu, G. Pan, Y. Zhang, Y. Shi, M. Guo and Y. Liu, *J. Memb. Sci.*, 2015, **475**, 504–510.

27 T. Fujioka, S. J. Khan, J. A. McDonald and L. D. Nghiem, *Desalination*, 2015, **368**, 69–75.

28 A.R.D.Verliefde, E.R.Cornelissen, S.G.J.Heijman, J.Q.J.C.Verberk, G.L.Amy, B.Van der Bruggen and J.C.van Dijk, *J. Memb. Sci.*, 2009, **339**, 10–20.

29 H. Ozaki, K. Sharma and W. Saktaywin, *Desalination*, 2002, **144**, 287–294.

30 S. Ding, Y. Yang, H. Huang, H. Liu and L. an Hou, *J. Hazard. Mater.*, 2015, **294**, 27–34.

31 T. Fujioka, L. D. Nghiem, S. J. Khan, J. A. McDonald, Y. Poussade and J. E. Drewes, *J. Memb. Sci.*, 2012, **409**–**410**, 66–74.

32 Y. Miyashita, S.-H. Park, H. Hyung, C.-H. Huang and J.-H. Kim, *J. Environ. Eng.*, 2009, **135**, 788–795.

33 B. Van Der Bruggen, J. Schaep, W. Maes, D. Wilms and C. Vandecasteele, *Desalination*, 1998, **117**, 139–147.

34 A. O. S. W.R. Bowen, *J. Colloid Interface Sci.*, 1994, **168**, 414–421.

35 Y. Kiso, T. Kon, T. Kitao and K. Nishimura, *J. Memb. Sci.*, 2001, **182**, 205–214.

36 I. Sutzkover, D. Hasson and R. Semiat, *Desalination*, 2000, **131**, 117–127.

37 S. Lee, G. Amy and J. Cho, *J. Memb. Sci.*, 2004, **240**, 49–65.

38 M. J. M. Wells, *Environ. Chem.*, , DOI:10.1071/EN06045.

39 L. D. Nghiem and P. J. Coleman, *Sep. Purif. Technol.*, 2008, **62**, 709–716.

40 K. C. Wijekoon, F. I. Hai, J. Kang, W. E. Price, W. Guo, H. H. Ngo, T. Y. Cath and L. D. Nghiem, *Bioresour. Technol.*, 2014, **159**, 334–341.

41 K. Kezia, J. Lee, A. J. Hill and S. E. Kentish, *J. Memb. Sci.*, 2013, **445**, 160–169.

42 K. L. Tu, A. R. Chivas and L. D. Nghiem, *J. Memb. Sci.*, 2014, **472**, 202–209.

580 43 K. O. Agenson, J. I. Oh and T. Urase, *J. Memb. Sci.*, 2003, **225**, 91–103.

581